Antagonistic cell surface and intracellular auxin signalling regulate plasma membrane H^+-fluxes for root growth

Lanxin Li
Institute of Science and Technology (IST) Austria
Inge Verstraeten
Institute of Science and Technology (IST) Austria
Mark Roosjen
Wageningen University
Koji Takahashi
Nagoya University
Lesia Rodriguez
Institute of Science and Technology (IST) Austria
Jack Merrin
Institute of Science and Technology (IST) Austria
Jian Chen
Ghent University
Lana Shabala
University of Tasmania
Wouter Smet
Ghent University
Hong Ren
University of Minnesota
Steffen Vanneste
Ghent University
Sergey Shabala
University of Tasmania
Bert De Rybel
Ghent University
Dolf Weijers
Wageningen University
Toshinori Kinoshita
Nagoya University
William M. Gray

University of Minnesota
Jiří Friml (Jiri.Friml@ist.ac.at)
Institute of Science and Technology (IST) Austria

Research Article

Keywords: auxin signalling, root growth, PM H⁺-ATPases, TMK1, Acid Growth Theory

Posted Date: September 2nd, 2021

DOI: https://doi.org/10.21203/rs.3.rs-266395/v2

Version of Record: A version of this preprint was published at Nature on October 27th, 2021. See the published version at https://doi.org/10.1038/s41586-021-04037-6.

Abstract

Growth regulation tailors plant development to its environment. A showcase is response to gravity, where shoots bend up and roots down[1]. This paradox is based on opposite effects of the phytohormone auxin, which promotes cell expansion in shoots, while inhibiting it in roots via a yet unknown cellular mechanism[2]. Here, by combining microfluidics, live imaging, genetic engineering and phospho-proteomics in *Arabidopsis thaliana*, we advance our understanding how auxin inhibits root growth. We show that auxin activates two distinct, antagonistically acting signalling pathways that converge on the rapid regulation of the apoplastic pH, a causative growth determinant. Cell surface-based TRANSMEMBRANE KINASE1 (TMK1) interacts with and mediates phosphorylation and activation of plasma membrane H^+-ATPases for apoplast acidification, while intracellular canonical auxin signalling promotes net cellular H^+-influx, causing apoplast alkalinisation. The simultaneous activation of these two counteracting mechanisms poises the root for a rapid, fine-tuned growth modulation while navigating complex soil environment.

Main

Auxin, a major growth regulator in plants, acts oppositely in shoots and roots. In shoots, canonical/intracellular auxin TRANSPORT INHIBITOR RESPONSE1 (TIR1)/AUXIN-SIGNALING F-BOX (AFB) receptors by downstream transcriptional regulation activate H^+-pumps to acidify the apoplast a promote cell elongation[3,4], in accordance with the Acid Growth Theory, which postulates that low apoplastic pH promotes growth[5]. In roots of many species including *Arabidopsis*, auxin inhibits growth. These contrasting responses are the basis for positive versus negative bending of roots and shoots in response to gravity and light[1]. The inhibitory auxin effect in roots also involves TIR1/AFB receptors but its rapid timing points towards an unknown non-transcriptional signalling branch[6]. Besides, a cell surface-based pathway involving TMK1 regulates development[7], including differential growth in the apical hook[8], while its role in auxin-regulated root growth remains unclear. Hence, the auxin signalling mechanism and the downstream processes for regulating root growth remain elusive.

In this study, we revealed antagonistic action of intracellular TIR1/AFB and cell surface TMK1 auxin signalling converging on regulation of apoplastic pH, which we confirm as the key cellular mechanism allowing immediate and sensitive root growth regulation.

Growth inhibition correlates with H^+-influx

Auxin rapidly inhibits root growth through a non-transcriptional branch of TIR1/AFB signalling[6]. Although several cellular processes, including cortical microtubule (CMT) reorientation[9,10], vacuolar fragmentation[11] and apoplastic pH changes[12-14] have been implicated, the causal mechanism remains unidentified.

We critically re-evaluated the kinetics of these processes using the vRootchip[6] (Extended Data Fig. 1a) in combination with vertical confocal microscopy[15]. Growth inhibition by 10nM natural auxin indole-3-acetic acid (IAA) was observed within 30s[6]. In contrast, less than 5% CMTs in elongating epidermal cells reoriented after 1min even at 100nM IAA and pharmacological inhibition of this reorientation had no effect on auxin-induced growth inhibition (Extended Data Fig. 1b-f). Similarly, we could not detect changes in vacuolar morphology in elongating cells even after 30min of 100nM IAA treatment (Extended Data Fig. 1g). These results argue against direct involvement of CMT reorientation and vacuole constriction in the rapid auxin-triggered growth inhibition.

To evaluate the kinetics of apoplastic pH, we applied a membrane-impermeable ratiometric pH indicator: 8-hydroxypyrene-1,3,6-trisulfonic acid (HPTS) and imaged apoplastic pH, while simultaneously tracking root tip growth. We detected an apoplastic pH gradient[12] in the root, decreasing from transition to elongation zone but regardless of their position, all cells showed a rapid (30s) apoplastic pH increase (Fig. 1a, b and Extended Data Fig. 2a). This provides higher temporal and spatial resolution to previous observations of auxin-induced apoplast alkalinisation[12] and reveals that auxin-triggered alkalinisation and root growth inhibition occur simultaneously (Fig. 1b). The pH increase was robust and extended to the external medium (Extended Data Fig. 2b). Using the *PM-Cyto* reporter for monitoring intracellular pH[16], we also detected simultaneous (30s) decrease in the PM-adjacent cytosolic pH after 5nM IAA treatment (Fig. 1c). Concomitant apoplastic increase and intracellular pH decrease implies H^+-influx into the cells. This was confirmed using non-invasive microelectrodes monitoring direct net H^+-exchange across the PM of elongating root epidermis cells after IAA treatment (Extended Data Fig. 2c), consistent with similar observations in root hair cells[17].

Overall, auxin triggers rapid apoplast alkalinisation by increasing the net cellular H^+-influx. Spatial and temporal correlation with root growth inhibition suggests apoplast alkalinisation as the underlying cellular mechanism.

Apoplastic pH regulates root growth

To investigate the causal relationship between apoplast alkalinisation and root growth inhibition, we manipulated the apoplastic pH by changing the medium pH (Extended Data Fig. 2d, e) and monitoring the impact on root growth. This extended previous observations of prolonged (2.5h) external extreme pH manipulation[12]. Replacement of the basal medium at pH 5.8 by more alkaline (pH 6.15) medium caused instant reduction of root growth; the growth rate restored rapidly after washout with the original pH 5.8 medium (Fig. 1d, e). Gradual alkalinisation of the medium resulted in gradual root growth inhibition (Extended Data Fig. 2f). Replacing basal medium by more acidic (pH 5.1) medium increased root growth instantly and washout restored original growth (Fig. 1f, g).

Thus, exogenous manipulation of apoplastic pH has immediate and reversible effects on root growth, with alkaline pH inhibiting and acidic pH promoting growth. This strongly supports that auxin-induced apoplast alkalinisation is the key downstream cellular mechanism for rapid root growth inhibition.

Auxin triggers PM H^+-ATPases activation

The auxin effect on apoplast alkalinisation occurs too fast to involve transcriptional regulation as also confirmed by pharmacological interference with translation (cycloheximide) or transcription (cordycepin) (Extended Data Figure 3a, b). To gain insights into the underlying mechanism, we mined recent datasets from Mass Spectroscopy (MS)-aided phospho-proteomics in WT root tips treated for 2min with 100nM IAA[18]. Among the differentially phosphorylated targets were two Plasma Membrane (PM) H^+-ATPases: AHA1 and AHA2. Multiple putative auxin-regulated phosphorylation sites were identified in the auto-inhibitory C-terminal region, leading to both activation and deactivation of H^+-pump activity[19] (Fig. 2a and Extended Data Table 1).

To test whether auxin changes the activity of PM H^+-ATPases in roots, we performed an ATP hydrolysis assay measuring the hydrolytic release of inorganic phosphate from ATP, representing the activity of PM H^+-ATPases. After 1h treatment with 100nM IAA, we detected increased ATP hydrolysis activity in root protein extracts (Fig. 2b). This suggests that auxin activates H^+-pumps, which should, however, lead to apoplast acidification instead of the observed alkalinisation (see Fig. 1b).

We next reanalysed the phospho-proteomics data specifically for the phosphorylation of Thr^{947} in AHA2, a well-known activation site[19]. Thr^{947} was significantly more phosphorylated after IAA treatment (Fig. 2c). To confirm this, we used an antibody against the AHA2 catalytic domain and the anti-pT947-AHA2 antibody revealing that 10nM IAA induced phosphorylation of Thr^{947} in 10min (Extended Data Fig. 3c). Thus, auxin induces AHA2 phosphorylation leading to its activation.

Our results show that auxin rapidly induces AHA phosphorylation leading to H^+-pump activation in roots. This is similar to shoots[20,21], however, is opposite to the observed auxin-induced H^+-influx (see Fig. 1), suggesting that in roots H^+-pump activation may act antagonistically to auxin-triggered apoplast alkalinisation.

H^+-ATPases counteract apoplast alkalinisation

To better understand the role of H^+-pump activation during auxin-triggered apoplast alkalinisation, we used the fungal toxin Fusicoccin (FC), which stabilizes the pump in the activated form[19] without affecting transcriptional auxin signalling (Extended Data Fig. 3d). FC caused rapid apoplast acidification and promoted root growth[12] (Extended Data Fig. 3e, f), opposite to auxin. When FC and IAA were applied

simultaneously or sequentially, we observed an intermediate response proportional to the auxin/FC ratio (Fig. 2d and Extended Data 3e-k). These suggest that FC-triggered H^+-ATPase activation and IAA-triggered apoplast alkalinisation act antagonistically.

To test this genetically, we analysed auxin response of loss- and gain-of-function *aha* mutants. Single *aha1* and *aha2* mutants showed no growth defects (Extended Data Fig. 3l), while the double mutant is embryo-lethal[19]. To overcome the redundancy, we used a synthetic trans-acting siRNA targeting *AHA1/2/7/11* (*AtTAS1c-AHA*), expressed from the *PIN2* promoter[22]. *AHAs* were downregulated in two independent transgenic lines (Extended Data Fig. 3m) and both were hypersensitive to auxin for apoplast alkalinisation (Fig. 2e) and root growth inhibition (Extended Data Fig. 3n). In contrast, constitutive activation of AHA1 in the *ost2-3D* mutant resulted in decreased auxin sensitivity of apoplastic pH (Fig. 2e) and root growth (Extended Data Fig. 3n).

These observation show that H^+-ATPase activation antagonizes auxin-induced apoplast alkalinisation in roots.

TMK1 interacts with H^+-ATPases

To address how auxin signalling regulates apoplastic pH, we performed co-immunoprecipitation (co-IP) followed by MS-assisted identification of proteins associated with either the TIR1/AFB1 receptor or PM-localized TMK1 auxin signalling component[7] (Extended Data Fig. 4a). For TIR1/AFB1 this approach did not reveal any relevant components, while for TMK1, AHAs were among the top enriched associated peptides (Extended Data Fig. 4b-d and Extended Data Table 2, 3).

We verified the interaction between AHAs and TMK1 by co-IP from *pTMK1::TMK1-FLAG* (Fig. 3a) and *pAHA2::AHA2-GFP* (Extended Data Fig. 4e) roots. From TMK1-FLAG pulldowns, we detected associated AHA2 and reciprocally from the AHA2-GFP pulldowns, we detected TMK1. Additional *in vivo* verification was provided by bimolecular fluorescent complementation (BiFC) in tobacco leaves co-transformed with TMK1 and AHA2 (Fig. 3b and Extended Data Fig. 4f).

These observations show that TMK1, the component of cell surface auxin signalling, interacts with PM H^+-ATPase.

TMK1 mediates auxin effect on H^+-ATPases

To test the role of TMK1 in H^+-ATPase phosphorylation, we performed phospho-proteomic analysis in *tmk1-1* roots compared to WT and detected strong hypo-phosphorylation of AHAs (Fig. 3c and Extended Data Table 1) suggesting TMK1 involvement in H^+-ATPases phosphorylation.

To verify this, we cloned *p35S::TMK1-HA* and two kinase-dead versions with mutations in the ATP binding site: *TMK1*^{K616E} or *TMK1*^{K616R}. Transient overexpression of the wild type (TMK1^{WT}), but not the kinase-dead constructs resulted in rapid wilting of tobacco leaves (Extended Data Fig. 5a), an effect consistent with PM H^+-ATPase activation[23]. We further generated *Arabidopsis* dexamethasone (DEX)-inducible gain-of-function lines. Compared to *TMK1*^{WT}, root extracts of *TMK1*^{K616R} did not show IAA-induced phosphorylation of AHA^{Thr947} (Extended Data Fig. 5b). Importantly, *in vitro* [g-^{32}P]-ATP kinase assays confirmed that TMK1^{WT}, but not kinase-dead TMK1^{K616E} directly phosphorylates the AHA2 C-terminal domain (Fig. 3d and Extended Data Fig. 5c).

Next, we analysed different *tmk* loss-of-function mutants. We detected less auxin-induced AHA2 phosphorylation in *tmk1-1* single, *tmk1,3* and the stunted *tmk1,4* double mutant roots (Fig. 3e and Extended Data Fig. 5d, e). Besides, the ATP hydrolysis assay showed that auxin-stimulated H^+-ATPase activity diminished in the *tmk1-1*, *tmk4-1* and *tmk1,4* roots (Fig. 3f).

Collectively, this demonstrates that active TMK1 mediates auxin-triggered phosphorylation and activation of H^+-ATPases in roots.

TIR1 and TMK1 converge on pH regulation

Our results show that TMK1 directly phosphorylates and activates PM H^+-ATPases leading to apoplast acidification (see Fig. 2 and 3). This is opposite to the observed auxin-induced apoplast alkalinisation leading to growth inhibition (see Fig. 1) prompting us to address the underlying signalling mechanism.

aux1-100 mutants in the auxin influx transporter AUXIN RESISTANT1 (AUX1) that are impaired in uptake of IAA[24] were less sensitive to auxin, both for growth inhibition[6] (Extended Data Fig. 6b, d) and apoplast alkalinisation (Extended Data Fig. 6a, c) suggesting requirement of intracellular auxin perception.

Given that intracellular TIR1/AFB receptors mediate auxin-triggered rapid growth inhibition[6], we evaluated apoplastic pH in parallel to growth in the *tir1 afb2 afb3* (*tir triple*) mutant. *tir triple* roots were resistant to IAA in both apoplast alkalinisation and growth inhibition (Fig. 4a and Extended Data Fig. 6e). AFB1 with its predominant cytosolic localization was proposed to be the major auxin receptor mediating auxin effect on growth and membrane depolarization[25,26]. We found that both TIR1 and AFB1 contribute to this regulation with *tir1-10* more auxin-resistant in the long term, while *afb1-3* showed pronounced resistance for rapid auxin effects (Extended Data Fig. 6h-k). We also applied the PEO-IAA anti-auxin to block downstream TIR1/AFB signalling[27]. Simultaneous addition of 10µM PEO-IAA and 5nM IAA prevented apoplast alkalinisation and growth inhibition (Extended Data Fig. 6f, g). We also took advantage of the cvxIAA/ccvTIR1 system, in which the engineered concave (ccv) TIR1 receptor cannot interact with natural IAA, but only with a synthetic convex (cvx) IAA, allowing specific activation of TIR1/AFB signalling[28]. Application of 50nM cvxIAA resulted in apoplastic alkalinisation in *ccvTIR1* plants (Fig. 4b), confirming

that specific activation of TIR1 is sufficient to trigger apoplast alkalinisation. These approaches demonstrate involvement of intracellular TIR1/AFB receptors in auxin-induced apoplast alkalinisation.

This effect is counteracted by the cell surface TMK1-mediated H^+-ATPase activation for apoplast acidification and growth promotion. Indeed, in the steady state, TMK1 is redundantly required for root growth as demonstrated by shorter roots in *tmk* mutants[7] (Extended Data Fig. 6l). In response to low concentrations of auxin, *tmk1*-related mutants were hypersensitive (Fig. 4c), while overexpressing TMK1 (*pUBQ10::TMK1-3HA*) led to a slight auxin resistance (Extended Data Fig. 6m). This resembles the corresponding loss- and gain-of-function *aha* mutants (see Fig. 2) providing additional support for the antagonistic, growth-promoting role of TMK-mediated AHA activity.

We also created a *tmk1 tir1* double mutant and analysed the auxin effect on apoplastic pH and root growth. As expected, *tmk1 tir1* mutants showed intermediate auxin sensitivity compared to the single mutants both for growth and apoplastic pH (Fig. 4d, e and Extended Data Fig. 6n, o).

Collectively, we propose that auxin activates two antagonistic signalling pathways: (i) cell surface TMK1-mediated H^+ export acidifying apoplast and (ii) more dominant, intracellular TIR1/AFB-dependent apoplast alkalinisation leading to rapid growth inhibition (Fig. 4f).

Conclusions

Our findings provide novel insights into a long-standing question how plant root growth is regulated. In particular, we address the old mystery of opposite growth regulation in shoots and roots by the phytohormone auxin and we also clarify the downstream cellular mechanism of auxin-triggered root growth inhibition.

Auxin regulates root growth very rapidly, utilizing a non-transcriptional branch of a signalling pathway downstream of intracellular TIR1/AFB receptors[6]. The same branch mediates apoplast alkalinisation, which we confirm as the causative cellular mechanism for root growth regulation, thus extending the classical Acid Growth Theory also for root growth inhibition.

Remarkably, auxin-induced apoplast alkalinisation in roots does not occur through regulation of PM H^+-ATPases as observed in shoots, where the TIR1/AFB transcriptional auxin signalling leads to PM H^+-ATPase activation and apoplast acidification[4,20]. Instead, in roots, PM H^+-ATPases are phosphorylated and activated by the cell surface TMK1-based auxin signalling, which leads to apoplast acidification. This mechanism, acts antagonistically to the more dominant TIR1/AFB-mediated alkalinisation.

A key open question concerns the downstream mechanism, by which TIR1/AFB signalling mediates apoplast alkalinisation. A plausible scenario would be a rapid increase in H^+ permeability across the PM, which is intertwined with changes in PM potential[25] (Extended Data Fig. 7a-c). Such auxin-triggered H^+-influx cannot be easily explained by $IAA^-/2H^+$ symport via the AUX1 influx carrier

as proposed[17] (Extended Data Fig. 7d) and seems to require previously reported[14] auxin-triggered cytosolic Ca^{2+} transients (Extended Data Fig. 8). Another persistent mystery is the auxin perception mechanism for the TMK1 pathway. Does this occur via direct activation of TMK1 by auxin or through another yet to be established auxin receptor?

With cell surface-based TMK1 activating H^+-pumps and intracellular TIR1/AFB signalling causing net cellular H^+-influx, two auxin-triggered mechanisms converge on regulation of extracellular pH, which directly determines root growth. This seemingly counterproductive simultaneous 'gas and brake' action presumably poises the root tip for rapid and flexible directional growth changes during the challenging task to navigate through complex soil environments.

Declarations

Acknowledgements

We thank Nataliia Gnyliukh and Lukas Hörmayer for technical assistance and Nadine Paris for sharing *PM-Cyto* seeds. We gratefully acknowledge Life Science, Machine Shop and Bioimaging Facilities *of IST Austria.* This project has received funding from the European Research Council Advanced Grant (ETAP-742985) and the Austrian Science Fund (FWF) I 3630-B25 to J.F., the National Institutes of Health (GM067203) to W.M.G., the Netherlands Organization for Scientific Research (NWO; VIDI-864.13.001.), the Research Foundation-Flanders (FWO; Odysseus II G0D0515N) and a European Research Council Starting Grant (TORPEDO-714055) to W.S. and B.D.R., the VICI grant (865.14.001) from the Netherlands Organization for Scientific Research to M.R and D.W., the Australian Research Council and China National Distinguished Expert Project (WQ20174400441) to S.S., the MEXT/JSPS KAKENHI to K.T. (20K06685) and T.K. (20H05687 and 20H05910), the European Union's Horizon 2020 research and innovation programme under the Marie Skłodowska-Curie Grant Agreement No. 665385 and the DOC Fellowship of the Austrian Academy of Sciences to L.L., the China Scholarship Council to J.C.

Author contributions.

L.L., I.V. and J.F. conceived and designed the experiments. L.L. and I.V. carried out most of the experiments and analysis. M.R. and D.W. performed the phospho-proteomics analysis and TIR1/AFB1 IP-MS/MS. I.V., W.S. and B.D.R. performed TMK1 IP-MS/MS experiments and statistical analysis. MS/MS analysis was performed by the VIB Proteomics Core. L.S. and S.S. performed MIFE experiments. K.T. and T.K. did the ATP hydrolysis assays. J.C. and S.V. created and shared the *AtTAS1c-AHA* lines. L.R. and L.L. created transgenic lines and crosses. H.R. and W.M.G. conducted [g-^{32}P]-ATP kinase assay, leaf wilting phenotype analysis, shared plasmids, seeds materials and contributed to discussion of the results. J.M. and L.L. modified the microfluidic chip. L.L., I.V. and J.F. wrote the manuscript.

Competing interests.

The authors declare no competing interests.

Correspondence

Additional information is available from the corresponding author upon request.

Data availability statement

The data and full blots are available within the paper and the Supplementary Information. All source data used for graphs are available.

Code availability statement

All codes used in the manuscript are provided in SI.

References

1 Estelle, M. Plant tropisms: the ins and outs of auxin. *Curr. Biol.* **6**, 1589-1591 (1996).

2 Gallei, M., Luschnig, C. & Friml, J. Auxin signalling in growth: Schrödinger's cat out of the bag. *Curr. Opin. Plant biol.* **53**, 43-49 (2020).

3 Spartz, A. K. *et al.* SAUR inhibition of PP2C-D phosphatases activates plasma membrane H^+-ATPases to promote cell expansion in Arabidopsis. *Plant Cell* **26**, 2129-2142 (2014).

4 Fendrych, M., Leung, J. & Friml, J. TIR1/AFB-Aux/IAA auxin perception mediates rapid cell wall acidification and growth of Arabidopsis hypocotyls. *Elife* **5**, e19048 (2016).

5 Du, M., Spalding, E. P. & Gray, W. M. Rapid auxin-mediated cell expansion. *Annu. Rev.Plant Biol.* **71**, 379-402 (2020).

6 Fendrych, M. *et al.* Rapid and reversible root growth inhibition by TIR1 auxin signalling. *Nat. Plants* **4**, 453 (2018).

7 Dai, N., Wang, W., Patterson, S. E. & Bleecker, A. B. The TMK subfamily of receptor-like kinases in Arabidopsis display an essential role in growth and a reduced sensitivity to auxin. *PloS One* **8**, e60990 (2013).

8 Cao, M. *et al.* TMK1-mediated auxin signalling regulates differential growth of the apical hook. *Nature* **568**, 240-243 (2019).

9 Chen, X. *et al.* Inhibition of cell expansion by rapid ABP1-mediated auxin effect on microtubules. *Nature* **516**, 90 (2014).

10 Adamowski, M., Li, L. & Friml, J. Reorientation of cortical microtubule arrays in the hypocotyl of Arabidopsis thaliana is induced by the cell growth process and independent of auxin signaling. *Int. J. Mol. Sci.* **20**, 3337 (2019).

11 Scheuring, D. *et al.* Actin-dependent vacuolar occupancy of the cell determines auxin-induced growth repression. *PNAS* **113**, 452-457 (2016).

12 Barbez, E., Dünser, K., Gaidora, A., Lendl, T. & Busch, W. Auxin steers root cell expansion via apoplastic pH regulation in Arabidopsis thaliana. *PNAS* **114**, E4884-E4893 (2017).

13 Monshausen, G. B., Miller, N. D., Murphy, A. S. & Gilroy, S. Dynamics of auxin-dependent Ca^{2+} and pH signaling in root growth revealed by integrating high-resolution imaging with automated computer vision-based analysis. *Plant J.* **65**, 309-318 (2011).

14 Shih, H.-W., DePew, C. L., Miller, N. D. & Monshausen, G. B. The cyclic nucleotide-gated channel CNGC14 regulates root gravitropism in Arabidopsis thaliana. *Curr. Biol.* **25**, 3119-3125 (2015).

15 Von Wangenheim, D. *et al.* Live tracking of moving samples in confocal microscopy for vertically grown roots. *Elife* **6**, e26792 (2017).

16 Martinière, A. *et al.* Uncovering pH at both sides of the root plasma membrane interface using noninvasive imaging. *PNAS* **115**, 6488-6493 (2018).

17 Dindas, J. *et al.* AUX1-mediated root hair auxin influx governs $SCF^{TIR1/AFB}$-type Ca^{2+} signaling. *Nat. Commun.* **9**, 1-10 (2018).

18 Han, H. *et al.* Rapid auxin-mediated phosphorylation of Myosin regulates trafficking and polarity in Arabidopsis. *bioRxiv* doi: https://doi.org/10.1101/2021.04.13.439603. (2021).

19 Haruta, M., Gray, W. M. & Sussman, M. R. Regulation of the plasma membrane proton pump (H^+-ATPase) by phosphorylation. *Curr. Opin. Plant Biol.* **28**, 68-75 (2015).

20 Takahashi, K., Hayashi, K.-i. & Kinoshita, T. Auxin activates the plasma membrane H^+-ATPase by phosphorylation during hypocotyl elongation in Arabidopsis. *Plant Phys.* **159**, 632-641 (2012).

21 Yang, Z. *et al.* TMK-based cell surface auxin signaling activates cell wall acidification in Arabidopsis. Research Square doi: 10.21203/rs.3.rs-203621/v1 (2021).

22 Zhang, Y., Xiao, G., Wang, X., Zhang, X. & Friml, J. Evolution of fast root gravitropism in seed plants. *Nat. Commun.* **10**, 1-10 (2019).

23 Kinoshita, T. & Shimazaki, K.-i. Analysis of the phosphorylation level in guard-cell plasma membrane H^+-ATPase in response to fusicoccin. *Plant Cell Physiol.* **42**, 424-432 (2001).

24 Yang, Y., Hammes, U. Z., Taylor, C. G., Schachtman, D. P. & Nielsen, E. High-affinity auxin transport by the AUX1 influx carrier protein. *Curr. Biol.* **16**, 1123-1127 (2006).

25 Serre, N. B. *et al.* AFB1 controls rapid auxin signalling through membrane depolarization in *Arabidopsis thaliana* root. *Nat. Plants,* 1-10 (2021).

26 Prigge, M. J. *et al.* Genetic analysis of the Arabidopsis TIR1/AFB auxin receptors reveals both overlapping and specialized functions. *Elife* **9**, e54740 (2020).

27 Hayashi, K.-i. *et al.* Rational design of an auxin antagonist of the SCF^{TIR1} auxin receptor complex. *ACS Chem. Biol.* **7**, 590-598 (2012).

28 Uchida, N. *et al.* Chemical hijacking of auxin signaling with an engineered auxin–TIR1 pair. *Nat. Chem. Biol.* **14**, 299 (2018).

Methods

Plant materials and growth conditions

All *Arabidopsis thaliana* mutants and transgenic lines used are in Columbia-0 (WT) background. The *pEB1b::EB1b-GFP*[1], *p35S::MAP4-GFP*[2], *pSYP22::SYP22-YFP*[3], *DR5::LUC*[4], *PM-Cyto*[5], *GCAMP*[6] marker lines were described previously. The *tir1-10*[7], *afb1-3*[8], *tir1-1 afb2-1 afb3-1* mutant[9], *pTIR1::ccvTIR1* in *tir1-1 afb2-3*[10], *pTIR1::TIR1* in *tir1-1 afb2-3* (we called it *control* for *ccvTIR1*)[10] and *aux1-100*[11], *cngc14-2*[12] were donated by the authors. The *pTIR1::TIR1-VENUS* in *tir1-1*[13], *pAFB1::AFB1-VENUS* in *afb1-3*[14] are shared by Stefan Kepinski. The *aha* mutants are the following: *aha2-5* (SALK_022010)[15], *aha1-7* (SALK_065288)[15], *ost2-3D*[16] shared by Atsushi Takemiya. Two independent lines *AtTAS1c-AHA#2* and *#4* were generated by Jian Chen and Steffen Vanneste as follows: the syn-tasiRNA target sequence was inserted into *pENTR-AtTAS1c-B/c*[17] using hybridized primers TAS-AHA pair (**Extended Data Table 4**) and was recombined into *pH7m24GW*[18] together with *pDONR P4-P1R*[19] carrying the *pPIN2* promoter[20], to generate *pPIN2:AtTAS1c-AHA*. The *pAHA2::AHA2-GFP*[21] seeds were donated by Anja T. Fuglsang. The *tmk* mutants are the following: *tmk3-2* (SALK_107741) ordered from NASC; Tongda Xu[22,23] kindly contributed *tmk1-1* (SALK_016360)*, tmk2-1* (SAIL_1242_H07), *tmk4-1* (GABI_348E01), the complemented *pTMK1::gTMK1-FLAG* in *tmk1-1* and *tmk1-1 tmk4-1* (*tmk1,4*) double mutant seeds. The *tmk1-1 tmk2-1* (*tmk1,2*) and *tmk1-1 tmk3-2* (*tmk1,3*) were generated by crosses using alleles above. The transgenic plant lines carrying *DEX::TMK1-HA* and *DEX-TMK1^{K616R}-HA* were generated by Hong Ren and William M. Gray. The

DEX::TMK1^{WT} (or TMK1$^{K616R/E}$)-HA constructs were done by cloning the cDNA of *TMK1^{WT}* (or *TMK1$^{K616R/E}$*) without stop codon (**Extended Data Table 4**) into *pENTR/D-TOPO*, and subsequently recombining into the *pBAV154*[24] binary vector used Gateway system. The *pUBQ10::gTMK1-3HA* and *pTMK1::gTMK1-eGFP* lines were generated by amplifying *TMK1* full length gDNA without stop codon from WT genomic DNA using the primers indicated in **Extended Data Table 4**. *TMK1* gDNA was inserted into *pDONR221,* subsequently recombined into *pB7m34GW* together with *pDONR P4-P1R* carrying the *UBQ10* or *TMK1* promoter and *pDONR P2R-P3 3xHA* or *pDONR P2R-P3 eGFP,* respectively. The constructs were transformed into the *Agrobacterium tumefaciens* strain pGV3101 by electroporation and further into WT plants by floral dip.

Seeds were surface-sterilized by chlorine gas, sown on half-strength Murashige and Skoog (½MS) medium supplemented with 1% (w/v) sucrose and 0.8% (w/v) phyto agar (pH 5.9), stratified in the dark at 4°C for 2d and then grown vertically at 21°C with a long-day photoperiod (16h light/8h dark). Light sources used were Philips GreenPower LED production modules [in deep red (660nm)/far red (720nm)/blue (455nm) combination, Philips], with a photon density of 140.4µmolm^{-2}s^{-1}±3%.

Treatment with inhibitors of gene translation, cycloheximide[25], or transcription, cordycepin[26] were done in the concentration and duration verified previously.

Microfluidics

The microfluidic vRootchip was used mostly to analyze root tip growth and apoplastic pH in real-time. The manufacturing of the chip, sample preparation procedure and data analysis of root tip growth were performed as described previously[25]. Our new design contains an additional valve in the control layer that closes the ends of the root channels (**Extended Data Fig. 1a**). In case of air bubbles appeared in the root channels, the additional valve allows pressurizing the channel and air will be absorbed into the Polydimethylsiloxane (PDMS) chip material within 2-10min. Afterwards, experiments started after adaptation of at least 2h. Besides, we introduced a graphical user interface (**Extended Data Script 1**) using the Processing software (https://processing.org/) with the ControlP5 package (http://www.sojamo.de/libraries/controlP5/) that sends serial commands to the Arduino. A sketch (**Extended Data Script 2**) runs on the Arduino to operate the electronics and receive commands. For one vRootchip, maximum 8 samples were used. When comparing two genotypes, 3-4 seedlings were used for each genotype and mounted in alternating channels to minimize the time difference between imaging two genotypes. For each root, we imaged one ROI containing early elongating epidermal cells and the other ROI covering the root tip. As these two ROIs were captured sequentially, we imaged the apoplastic pH and the growth of the same root close to simultaneously.

In vRootchip, we used basal liquid medium ¼MS+0.1% sucrose, pH 5.8 (adjusted with KOH). The media of different pH was prepared with basal medium adjusted pH by HCl or KOH. Besides, Ca^{2+}-free liquid

medium was prepared without $CaCl_2$.

Scanner growth assay

To complement the real-time imaging in vRootchip, growth analysis was performed on a vertical scanner with bigger sample sizes allowing more conditions to be evaluated. This growth measurement we called steady-state. 4d-old seedlings were transferred to 60×15mm petri dishes filled with 5ml ½MS medium with treatments as indicated. The petri dishes were placed on a vertically mounted flatbed scanner (Epson perfection V370) and seedlings were imaged through the layer of medium. Either wet black filter paper or ½MS medium containing activated charcoal was added in the lid to improve background contrast. The samples were automatically imaged every 10 or 30min using the AutoIt script described previously[27] and scans were taken at 1200dpi. The resulting image series were analyzed using StackReg stabilization and the Manual Tracking plugin in ImageJ, or using an in-house generated MATLAB-based application RootGrowth tracker[28].

Imaging and measuring apoplastic pH with HPTS dye

All apoplastic pH data were obtained using 8-hydroxypyrene-1,3,6-trisulphonic acid (HPTS), a ratiometric fluorescent pH dye[29]. pH measurements were done both in steady-state condition and real-time vRootchip imaging. For steady-state pH analysis, 4d-old seedlings were transferred to ½MS medium containing 1mM HPTS (Thermo Scientific 6358-69-6, dissolved in ddH_2O) and treatments were performed for 30 or 50min. Subsequently, seedlings on a slice of the treatment medium were mounted into a Lab-Tek Chambered Coverglass.

Real-time imaging of the apoplastic pH was done in vRootchip containing medium (¼MS+0.1% sucrose) supplemented with 1mM HPTS with or without treatment. All imaging was performed on the in-house established vertical Zeiss LSM 800 confocal microscope[30]. Fluorescent signals for protonated HPTS (excitation 405nm, emission 514nm, visualized in red) and deprotonated HPTS (excitation, 488nm, emission 514nm, visualized in green) were detected with a 20x/0.8 air objective. Image analysis was performed on a cropped region of elongating epidermis cells using batch processing of a previously described the ImageJ macro[29]. Relative pH value is calculated as the background-subtracted intensity of the deprotonated intensity divided by that of the protonated intensity. Resulting relative pH data were plotted over time and statistically evaluated in GraphPad Prism 6. Note that we did not transform the relative pH value to absolute pH values, which would require the generation of a calibration curve for each experiment.

Imaging and measuring cytosolic pH with *PM-cyto* reporter

Real-time imaging of the cytosolic pH near the PM was done by using *PM-Cyto* reporter line[5] in vRootchip and a vertical Zeiss LSM 800 confocal microscope[30]. Sequential illumination at 488 and 405nm with emission 514nm for both, corresponding to the two absorption peaks of pHluorin, were taken with a 20x/0.8 air objective. For each root in vRootchip, two ROIs were tracked over time with one containing elongating epidermal cells for measuring the cytosolic pH and the other covering the root tip for measuring the root growth rate. Image analysis was performed similar to the HPTS analysis described above.

Imaging microtubule orientation, vacuolar morphology and cytosolic Ca^{2+} spike

The *pEB1b::EB1b-GFP* maker line[1] was used to track the dynamics of CMTs orientation in vRootchip. Images were obtained every 6.25s and the analysis of the CMTs orientation was done in ImageJ by max Z-projection on every 10 frames and quantification by a for batch processing modified version of the Fibril Tool macro[31]. The *p35S::MAP4-GFP* marker line[2] was used for capturing the CMTs orientation after treatment for the indicated time period (steady state). The CMTs orientation angle was calculated using the Bioline script[32]. For both marker lines, the GFP (excitation 488nm, emission514 nm) signal was detected by Plan-Apochromat 20x/0.8 air objective in the vertical Zeiss LSM 800 confocal microscope[30].

The *pSYP22::SYP22-YFP* marker line[3] was used for imaging vacuolar morphology. We used a mounting system[33], which allows the injection of new liquid medium during imaging. Images were taken before and 30min after Mock or 100nM IAA treatment and the YFP (excitation 488 nm, emission 527 nm) intensity was detected with C-Apochromat 40x/1.20 W Korr objective in an inverted Zeiss LSM 800 confocal microscope.

The *GCaMP* marker line[6] was crossed into *ccvTIR1* and *control* transgenic plants[10] and used for imaging cytoslic Ca^{2+} level in vRootchip. Images were taken every 14.4s for 1h. GFP (excitation 488nm, emission 514 nm) signal was detected by Plan-Apochromat 20x/0.8 air objective in the vertical Zeiss LSM 800 confocal microscope[30].

Non-invasive microelectrode (MIFE) ion flux measurements

Net fluxes of H^+, K^+, and Ca^{2+} were measured using the non-invasive microelectrode ion flux estimation (MIFE) technique essentially as described elsewhere[34]. In brief, microelectrodes were pulled out by PE-22 puller (Narishige), dried in an oven and silanized with tributylchlorosilane (Cat 90794, Sigma-Aldrich, Australia). The prepared electrode blanks were backfilled with respective solutions for each measured ion and electrode tips front-filled with selective liquid ion exchangers (LIX) purchased from Sigma-Aldrich) to

measure ions of interest (H^+ - Cat. 95291; K^+- Cat. 99311, Ca^{2+}- Cat. 99310). A root of intact 6d-old *Arabidopsis* WT seedlings was immobilised in a measuring chamber using Perspex holders and basic salt media (BSM) added. The composition of the BSM solution was 0.5mM KCl and 0.1mM $CaCl_2$; pH 5.8, unbuffered. Measurements were recorded from root elongating epidermal cells (~450µm from the root tip). After 40min of conditioning, the microelectrodes were positioned 20µm from the root surface and moved in a slow (6s cycle, 100µm amplitude) square-wave by a computer-driven micromanipulator (MHW-4, Narishige). Net ion fluxes were calculated by the MIFEFLUX software based on the measured difference in electrochemical gradient between these two positions using the cylindrical diffusion geometry as described elsewhere[34]. The steady fluxes were recorded for 5-10min to make sure that steady state condition was reached. Then 10nM IAA was applied to the measuring chamber, and transient H^+, K^+, and Ca^{2+} kinetics were measured for further 20min. At least 9 individual plants from several batches were used. The sign convention is “influx positive”.

Membrane potential measurements

Membrane potential (MP) values were measured from root epidermal elongating cells of intact Arabidopsis seedlings. Conventional microelectrodes (Harvard Apparatus) were filled with 1M KCL and connected to the MIFE electrometer via the Ag/AgCl half-cell. During MP measurement, the microelectrode with a tip diameter of 0.5µm was manually impaled into the epidermal cells of elongation (~450µm from root tip) using a 3D-micromanipulator (MHW-4, Narishige). MP values were recorded by the MIFE CHART software for at least two minutes after stabilization[34]. Prior to measurements, a 6d-old seedling was immobilised on a Perspex block using Parafilm strips, the block then was inserted into a vertical Perspex measuring chamber and filled with basic salt media (BSM: 0.5mM KCl and 0.1mM CaCl2; unbuffered, of required pH). After 40min conditioning in BSM, the measuring chamber was mounted on a MIFE microscope stage located in a Faraday cage for MP measurements. MP measurements were conducted in two ways: under steady state conditions (at different pH values) and as transient kinetics (in response to IAA application). In the steady state experiments, MP values were recorded from roots of 5-6 individual seedlings with a new electrode being used for each measurement to ensure that the electrode tip was not blocked. At least 4 measurements were made for each seedling. In transient kinetics experiments, MP was recorded from a root in BSM (pH 5.8) for 1-2min after the initial cell penetration and then IAA prepared in BSM was added to the chamber (final concentration 10nM) followed by 5min MP recording.

Evaluating the TIR1-transcriptional response using *DR5::LUC*

4d-old *DR5::LUC* seedlings[4] are placed on the surface of solidified ½MS medium with 200µl of 5mM D-luciferin dissolved in a 1x PBS drop on the root tips for 30min as pre-treatment. Subsequently, the

samples were transferred to solidified ½MS medium supplemented with mock, 10nM IAA, 10µM FC and IAA+FC, and immediately imaged in an in-house established dark box with a Photometric Evolve® EMCCD camera equipped with a 17mm fixed lens/0.95 and an additional 125mm lens[27]. The multiplier EMCCD gain was set to 70s and the exposure time to 35s, and images were acquired every 2min. The resulting time-lapse video was analysed in ImageJ as described previously[27].

Identification of TMK1-interacting proteins using IP/MS-MS

Immunoprecipitation (IP) experiments were performed in 3 biological replicates as described previously[35] using 1g of roots of 7d-old seedlings from the *pTMK1::TMK1-eGFP* transgenic line and 1g of roots from WT. Interacting proteins were isolated by incubating total protein extracts with 100µL anti-GFP coupled magnetic beads (Miltenyi Biotech). 3 replicates of *pTMK1::TMK1-eGFP* were compared to 3 WT replicates. Tandem mass spectrometry (MS) on a Q-Exactive device (Thermo Fisher) and statistical analysis using MaxQuant and Perseus software was performed as described previously[36].

Identification of TIR1- and AFB1-interacting proteins using IP/MS-MS

For immunoprecipitation, ground plant material of *pTIR1::TIR1-VENUS* in *tir1-1* and *pAFB1::AFB1-VENUS* in *afb1-3* transgenic lines was lysed in mild lysis buffer (50mM Tris pH 7.5, 150mM NaCl, 2mM $MgCl_2$, 0.2mM EDTA, 1xCPI, 0.5mM DTT, 0.2% NP40 and 1mg/ml DNAse) and mildly sonicated using a Bioruptor (Diagenode). After lysate clearance, supernatant was submitted to enrichment using GFP-Trap agarose beads (Chromotek) for 45min at 4°C while gently rotating. Beads were subsequently washed twice in lysis buffer, twice in detergent-free lysis buffer and trice in 50mM Ammoniumbicarbonate (ABC) (Sigma) with intermediate centrifuging for 2min at 2000g at 4°C. After the final wash, bead-precipitated proteins were alkylated using 50mM Acrylamide (Sigma). Precipitated proteins were submitted to on-bead trypsin digestion using 0.35µg trypsin (Roche) per reaction. After overnight incubation at 25°C, peptides were desalted and concentrated using C18 Stagetips.

After Stagetip processing, peptides were applied to online nanoLC-MS/MS using a 60min acetonitrile gradient from 8-50%. Spectra were recorded on a LTQ-XL mass spectrometer (Thermo Scientific) and the statistical analysis using MaxQuant and Perseus software was performed as described previously[36].

Phospho-proteomics of auxin-treated roots

Roots from 5d-old plants were treated and immediately harvested and flash frozen in liquid nitrogen. They then were ground to fine powder in liquid nitrogen. Powder was suspended in SDS lysis buffer (100mM Tris pH 8.0, 4%SDS and 10mM DTT) and sonicated using a cooled Biorupter (Diagenode) for

10min using high power with 30s on 30s off cycle. Lysate was cleared by centrifugation at maxiumum speed for 30min. Protein concentrations were determined using the Bradford reagent (Bio-Rad).

For FASP 30kDa cut-off amicon filter units (Merck Millipore) were used. Filters were first tested by appling 50µl urea buffer UT buffer (8M Urea and 100mM Tris pH 8.5) and centrifuging for 10min at 11000rpm at 20°C. The desired amount of protein sample was next mixed with UT buffer until a volume of 200µl, applied to filter and centrifuged for 15min. All centriguge steps were at 11000rpm at 20°C. Filter was washed with UT buffer for 15 min. Retained proteins were alkylated with 50mM acrylamide (Sigma) in UT buffer for 30min at 20°C while gently shaking followed by a triple wash step with UT buffer for 15 minutes and three washes with 50mM ABC buffer. After last wash proteins were cleaved by adding trypsin (Roche) in a 1:100 trypsin to protein ratio. Digestion was completed overnight. The following day filter was changed to a new tube and peptides were eluted by centrifuging for 15min. Further elution was completed by adding two times 50mM ABC buffer and centrifuging for 10min on 11000rpm at 20°C.

For peptide desalting and concentrating 200 µl tips were fitted with 2 plugs of C18 octadecyl 47mm Disks 2215 *(Empore™)* material and 1mg:10µg of LiChroprep® RP-18:peptides (Merck). Tips were sequentially equilibrated with 100% methanol, 80% ACN in 0.1% formic acid and twice with 0.1% formic acid for 4min at 1500g. After equilibration peptides were loaded for 20min at 400g. Bound peptides were washed with 0.1% formic acid and eluted with 80% ACN in 0.1% formic acid for 4min at 1500g. Eluted peptides were subsequently concentrated using a vacuum concentrator for 30min at 45°C and resuspended in 50µl of 0.1% formic acid.

For phosphopeptide enrichment magnetic Ti^{4+}-IMAC (MagResyn) were used according to manufactures protocol. Enrichments were perfromed with 1mg of peptides in biological quadruplicate.

After Stagetip processing, peptides were applied to online nanoLC-MS/MS using a 120min acetonitrile gradient from 8-50% for phospho-proteomics. Spectra recording and statistical analysis were as previously described, with the addition of phosphorylation as a variable modification[36]. Filtering of datasets was done in Perseus in as described[37].

Phospho-proteomics in WT and *tmk1-1* roots

4 biological replicates of WT and *tmk1-1* roots were prepared and treated as indicated above. They were submitted to the phospho-proteomic pipeline[36,37] and differentially phosphorylated peptides belonging to H^+-ATPases were specifically filtered out of the big dataset (**Extended Data Table 1**).

in vitro kinase assay with [g-^{32}P]-ATP

6xHis-MBP-$TMK1^{WT}$ kinase domain (or kinase-dead $TMK1^{K616E}$) was purified from *E. coli*. Briefly, ca. 100ng of purified protein was added to reactions containing 5 mM HEPES, pH 7.5, 10 mM $MgCl_2$, 10mM

$MnCl_2$, 1mM DTT and the assay initiated by adding 1µl of ATP solution containing 100µM (unlabeled) ATP and 33nM [g-^{32}P]-ATP (3000 Ci/mmol). ca. 150ng of purified GST-AHA2 C-terminal was added as indicated. Reactions were incubated at 28°C for 40min, stopped with SDS-PAGE sample buffer, run out on SDS-PAGE and phosphorylation was visualized by autoradiography. Ponceau staining was performed as loading control.

Protein extraction and Western blot analysis for co-IP and determination of AHA2 phosphorylation state

To isolate PM H^+-ATPases and potential interactors, 5-7d-old plant roots were harvested at the indicated time points after 10 or 100nM IAA auxin treatment. 24h prior to the evaluation of auxin effects, these seedlings were sprayed with ½AM solution containing 30µM kynurenine. The root samples were flash frozen in liquid nitrogen and ground (Retsch mill, 2x 1min at 20Hz). The root powder was then resuspended in a 1:1 (w/v) ratio in protein extraction buffer (25mM Tris-HCl, pH 7.5, 150mM NaCl, 1% Triton X-100, 1xRoche cOmplete™ Protease Inhibitor Cocktail, 1xRoche PhosSTOP™, 1mM EDTA, 1mM DTT and 0.5mM PMSF). The samples were incubated on ice for 30min, followed by a centrifuging step at 10000*g* to discard the plant debris. The cleared supernatant containing the proteins of interest was collected and the total protein content was determined using Quick Start Bradford reagent (Bio-Rad). This could further be used for co-immunoprecipitation analysis or for SDS-PAGE analysis. In order not to lose relevant proteins, protein samples were not boiled in the presence of reducing Laemmli buffer and no harsher PM extraction or membrane enrichment was attempted.

For co-immunoprecipitation, root extracts (obtained by extraction in the Lysis buffer supplied in the Miltenyi µMACs kit, supplemented with 1xRoche cOmplete™ Protease Inhibitor Cocktail, 1mM DTT and 0.5mM PMSF), were incubated with magnetic beads from the Miltenyi anti-GFP, anti-HA or anti-FLAG µMACs kits (depending on the tags of the proteins of interest) and kept rotating for 4h at 4°C. Elution was performed with room-temperature denaturing elution buffer and the proteins were analyzed by SDS-PAGE and Western blot.

Following separation of proteins by SDS-PAGE in a 10% acrylamide gel (Protean® TGX™, Bio-Rad), proteins were transferred to PVDF membranes by electroblotting (Trans-blot® Turbo™, Bio-Rad). The membranes were then incubated in blocking buffer (0.05% Tween-20, 5% milk powder or 3% BSA, 20mM Tris-HCl, pH 7.5 and 150mM NaCl) for at least 60min and incubated with antibody solution against the protein of interest. All raw gel data are shown in **Supplemental Information**.

Antibodies

The anti-AHA2 and anti-Thr^{947} AHA2 antibody were shared by Toshinori Kinoshita and used as described previously[38] at final dilution of 1:5000 in TBST buffer+3% BSA, followed by anti-rabbit IgG secondary

antibody conjugated to horseradish peroxidase (HRP) (GE Healthcare, NA934) at a dilution of 1:10000 and chemiluminescence reaction (SuperSignal West Femto, Thermo Scientific). To allow multiple antibody detections using the same PVDF membrane, mild stripping was performed using 15g/L glycine, 1g/L SDS, 10mL/L Tween-20 buffer at pH 2.2 for 2-5min.

ATP hydrolysis in root samples

To deplete endogenous auxin levels in the seedlings, 14d-old plants were pre-treated with 30μM kynurenine for 24h in the dark. Then, the pretreated seedlings were incubated in presence and absence of 100nM IAA for 60min under dark condition. The roots excised from the seedlings were homogenized in homogenization buffer (50mM MOPS-KOH,pH 7.0, 100mM KNO_3, 2mM sodium molybdate, 0.1mM NaF, 2mM EGTA, 1mM PMSF and 20μM leupeptin) and the homogenates were centrifuged at 10000*g* for 10min. The obtained supernatant was further ultra-centrifuged at 45000 rpm for 60min. The resultant precipitate (microsomal fraction) was resuspended in the homogenization buffer. ATP hydrolytic activity in the microsomal fraction was measured by the release of inorganic phosphate from ATP in a vanadate-sensitive manner following the method published[39] with the following modifications. The microsomal fraction (22.5μL, 0.2mg/mL) was mixed with the equal volume of the reaction buffer (60mM MES-Tris. pH 6.5, 6mM $MgSO_4$, 200mM KNO_3, 1 mMammonium molybdate, 10μg/mL oligomycin, 2mM NaN_3, 0.1% Triton X-100, 1mM PMSF and 20μM leupeptin) with or without 1μL of 10mM sodium orthovanadate. The reaction was started by adding 5μL of 2mM ATP and terminated by adding 50μL of the stop solution (2.6% [w/v] SDS, 0.5% [w/v] sodium molybdate and 0.6N H_2SO_4) after incubating at 30ºC for 30min.

Bimolecular Fluorescence Complementation (BiFC)

Following the method described[40], the full-length coding sequences of AHA2 and TMK1 without stop codons were amplified by PCR (primers in **Extended Data Table 4**), cloned into *pENTR/D-TOPO* or *pDONR207* and recombined in *pSPYNE* and *pSPYCE*[41] to generate BiFC expression constructs. The resulting binary vectors were introduced in *Agrobacterium* GV3101 by electroporation and these were cultured until OD_{600} 0.8. Syringe infiltration was performed in *Nicotiana benthamiana* leaves as described[42]. For the constructs of interest, final OD_{600} of 0.2 was used and p19 was co-infiltrated at OD_{600} 0.1 to avoid gene silencing. Infiltration buffer of pH 5.8 contained: 10mM $MgSO_4$, 10mM MES-KOH and 0.15mM acetosyringone. TMK1 overexpression, even transiently, has a strong effect on the viability of the leaves, so samples were taken daily after infiltration to determine the optimal balance between expression level and viable leaf cells. To visualize protein interactions, sections of the leaves were imaged using a Zeiss LSM 700 confocal microscope.

Quantitative RT-PCR

RNA was extracted from 5d-old light-grown root tips with the RNAeasy Plant Mini Kit (Qiagen), with three biological replicates for each genotype. 2µg of RNA was used for cDNA synthesis (Qiagen). Samples were pipetted in three technical replicates using an automated JANUS Workstation (PerkinElmer) and measured by the Real-time PCR Roche LightCycler 480 using Luna® Universal qPCR mastermix (NEB, M3003S). Primers utilized for assessing gene expression are listed in Extended Table 4. Expression levels were normalized to Elongation factor 1-alpha (At5G60390)[43].

Statistical analysis and reproducibility

All graphs were generated using GraphPad Prism 6 or 8. For statistical analysis of vRootchip data, Two-way ANOVA was performed for the entire time frame of the experiment, except when a specific time interval is indicated. Welch ANOVA analysis was applied for the scanner growth assay with multiple time points, and one-way ANOVA assays were used for steady state (one incubation time point) pH and scanner growth datasets. Stars indicate significant differences on all graphs with ns for $p>0.05$, * for $p\leq0.05$, ** for $p\leq0.01$, *** for $p\leq0.001$ and **** for $p\leq0.0001$. Experiments always included sufficient biological replicates and were repeated at least twice independently with similar results. The depicted data show the results from one representative experiment.

Methods and Extended Data Figure references

1 Komaki, S. *et al*. Nuclear-localized subtype of end-binding 1 protein regulates spindle organization in Arabidopsis. *J. Cell Sci* **123**, 451-459 (2010).

2 Marc, J. *et al.* A GFP–MAP4 reporter gene for visualizing cortical microtubule rearrangements in living epidermal cells. *Plant Cell* **10**, 1927-1939 (1998).

3 Robert, S. *et al.* Endosidin1 defines a compartment involved in endocytosis of the brassinosteroid receptor BRI1 and the auxin transporters PIN2 and AUX1. *PNAS* **105**, 8464-8469 (2008).

4 Moreno-Risueno, M.A. *et al*. Oscillating gene expression determines competence for periodic Arabidopsis root branching. *Science* **329**, *1306-11 (2010)*

5 Martinière, A. *et al*. Uncovering pH at both sides of the root plasma membrane interface using non-invasive imaging. *PNAS*, **115**, 6488-6493 (2018).

6 Toyota, M. *et al*. Glutamate triggers long-distance, calcium-based plant defense signaling. *Science* 361, 1112-1115 (2018).

7 Parry, G. *et al*. Complex regulation of the TIR1/AFB family of auxin receptors. *PNAS* **106**, 22540-22545 (2009).

8 Prigge, M. J. et al. Genetic analysis of the Arabidopsis TIR1/AFB auxin receptors reveals both overlapping and specialized functions. *Elife* **9**, e54740 (2020).

9 Dharmasiri, N. *et al.* Plant development is regulated by a family of auxin receptor F box proteins. *Dev. Cell* **9**, 109-119 (2005).

10 Uchida, N. *et al.* Chemical hijacking of auxin signaling with an engineered auxin–TIR1 pair. *Nat. Chem. Biol.* **14**, 299 (2018).

11 Swarup, R. *et al.* Structure-function analysis of the presumptive Arabidopsis auxin permease *AUX1*. *Plant Cell* **16**, 3069-3083 (2004).

12 Shih, H.-W., DePew, C. L., Miller, N. D. & Monshausen, G. B. The cyclic nucleotide-gated channel CNGC14 regulates root gravitropism in Arabidopsis thaliana. *Curr. Biol.* **25**, 3119-3125 (2015).

13 Wang, R. *et al.* HSP90 regulates temperature-dependent seedling growth in Arabidopsis by stabilizing the auxin co-receptor F-box protein TIR1. *Nat. Commun.* **7**, 1-11 (2016).

14 Rast-Somssich, M. I. *et al.* The Arabidopsis *JAGGED LATERAL ORGANS* (*JLO*) gene sensitizes plants to auxin. *J. Exp. Bot.* **68**, 2741-2755 (2017).

15 Haruta, M. *et al.* Molecular characterization of mutant Arabidopsis plants with reduced plasma membrane proton pump activity. *J. Biol. Chem.* **285**, 17918-17929 (2010).

16 Yamauchi, S. *et al.* The plasma membrane H^+-ATPase AHA1 plays a major role in stomatal opening in response to blue light. *Plant Phys.* **171**, 2731-2743 (2016).

17 Carbonell, A. *et al.* New generation of artificial microRNA and synthetic trans-acting small interfering RNA vectors for efficient gene silencing in Arabidopsis. *Plant Phys.* **165**, 15-29 (2014).

18 Karimi, M., Bleys, A., Vanderhaeghen, R. & Hilson, P. Building blocks for plant gene assembly. *Plant Phys.* **145**, 1183-1191 (2007).

19 Marquès-Bueno, M. M. *et al.* A versatile multisite gateway-compatible promoter and transgenic line collection for cell type-specific functional genomics in Arabidopsis. *Plant J.* **85**, 320-333 (2016).

20 Zhang, Y., Xiao, G., Wang, X., Zhang, X. & Friml, J. Evolution of fast root gravitropism in seed plants. *Nat. Commun.* **10**, 1-10 (2019).

21 Fuglsang, A. T. *et al.* Receptor kinase-mediated control of primary active proton pumping at the plasma membrane. *Plant J.* **80**, 951-964 (2014).

22 Cao, M. *et al.* TMK1-mediated auxin signalling regulates differential growth of the apical hook. *Nature* **568**, 240 (2019).

23 Wang, Q. *et al.* A phosphorylation-based switch controls *TAA1*-mediated auxin biosynthesis in plants. *Nat. Commun.* **11**, 1-10 (2020).

24 Lee, J. *et al.* Type III secretion and effectors shape the survival and growth pattern of *Pseudomonas syringae* on leaf surfaces. *Plant Phys.* **158**, 1803-1818 (2012).

25 Fendrych, M. *et al.* Rapid and reversible root growth inhibition by TIR1 auxin signalling. *Nat. Plants* **4**, 453 (2018).

26 Robert, S. *et al*. ABP1 mediates auxin inhibition of clathrin-dependent endocytosis in Arabidopsis. *Cell* **143**, 111-121 (2010).

27 Li, L., Krens, S. G., Fendrych, M. & Friml, J. Real-time analysis of auxin response, cell wall pH and elongation in Arabidopsis thaliana hypocotyls. *Bio Protoc.* **8** (2018).

28 Gelová, Z. *et al*. Developmental roles of auxin binding protein 1 in Arabidopsis Thaliana. *Plant Sci.* **303**, 110750 (2021).

29 Barbez, E., Dünser, K., Gaidora, A., Lendl, T. & Busch, W. Auxin steers root cell expansion via apoplastic pH regulation in *Arabidopsis thaliana*. *PNAS* **114**, E4884-E4893 (2017).

30 Von Wangenheim, D. *et al.* Live tracking of moving samples in confocal microscopy for vertically grown roots. *Elife* **6**, e26792 (2017).

31 Boudaoud, A. *et al.* FibrilTool, an ImageJ plug-in to quantify fibrillar structures in raw microscopy images. *Nat. Protoc.* **9**, 457-463 (2014).

32 Adamowski, M., Li, L. & Friml, J. Reorientation of cortical microtubule arrays in the hypocotyl of *Arabidopsis thaliana* is induced by the cell growth process and independent of auxin signaling. *Int. J. Mol. Sci.* **20**, 3337 (2019).

33 Narasimhan, M. et al. Systematic analysis of specific and nonspecific auxin effects on endocytosis and trafficking. *Plant Phys.* **186**, 1122-1142 (2021).

34 Shabala, S. N., Newman, I. A. & Morris, J. Oscillations in H^+ and Ca^{2+} ion fluxes around the elongation region of corn roots and effects of external pH. *Plant Phys.* **113**, 111-118 (1997).

35 De Rybel, B. *et al.* A bHLH complex controls embryonic vascular tissue establishment and indeterminate growth in Arabidopsis. *Dev. Cell* **24**, 426-437 (2013).

36 Wendrich, J. R., Boeren, S., Möller, B. K., Weijers, D. & De Rybel, B. in *Plant Hormones*: 147-158 (Springer, 2017).

37 Nikonorova, N. *et al.* Early mannitol-triggered changes in the Arabidopsis leaf (phospho)proteome reveal growth regulators. *J. Exp. Bot.* **69**, 4591-4607 (2018).

38 Hayashi, Y. *et al.* Biochemical characterization of in vitro phosphorylation and dephosphorylation of the plasma membrane H^+-ATPase. *Plant Cell Physiol.* **51**, 1186-1196 (2010).

39 Inoue, S.-i., Takahashi, K., Okumura-Noda, H. & Kinoshita, T. Auxin influx carrier AUX1 confers acid resistance for Arabidopsis root elongation through the regulation of plasma membrane H^+-ATPase. *Plant Cell Physiol.* **57**, 2194-2201 (2016).

40 Spartz, A. K. *et al.* SAUR inhibition of PP2C-D phosphatases activates plasma membrane H^+-ATPases to promote cell expansion in Arabidopsis. *Plant Cell* **26**, 2129-2142 (2014).

41 Walter, M. *et al.* Visualization of protein interactions in living plant cells using bimolecular fluorescence complementation. *Plant J.* **40**, 428-438 (2004).

42 Leuzinger, K. *et al*. Efficient agroinfiltration of plants for high-level transient expression of recombinant proteins. *J. Vis. Exp.* **77**: 50521 (2013).

43 Czechowski, T., Stitt, M., Altmann, T., Udvardi, M. K. & Scheible, W.-R. Genome-wide identification and testing of superior reference genes for transcript normalization in Arabidopsis. *Plant Phys.* **139**, 5-17 (2005).

44 Serre, N. B. et al. AFB1 controls rapid auxin signalling through membrane depolarization in *Arabidopsis thaliana* root. *Nat. Plants,* 1-10 (2021).

45 Dindas, J. *et al*. AUX1-mediated root hair auxin influx governs $SCF^{TIR1/AFB}$-type Ca^{2+} signaling. *Nat. Commun.* **9**, 1-10 (2018).

46 Yang, Y., Hammes, U. Z., Taylor, C. G., Schachtman, D. P. & Nielsen, E. High-affinity auxin transport by the AUX1 influx carrier protein. *Curr. Biol* **16**, 1123-1127 (2006).

47 Dumont, J. N. Oogenesis in Xenopus laevis (Daudin). I. Stages of oocyte development in laboratory maintained animals. *J. Morphol* **136**, 153-179 (1972).

Figures

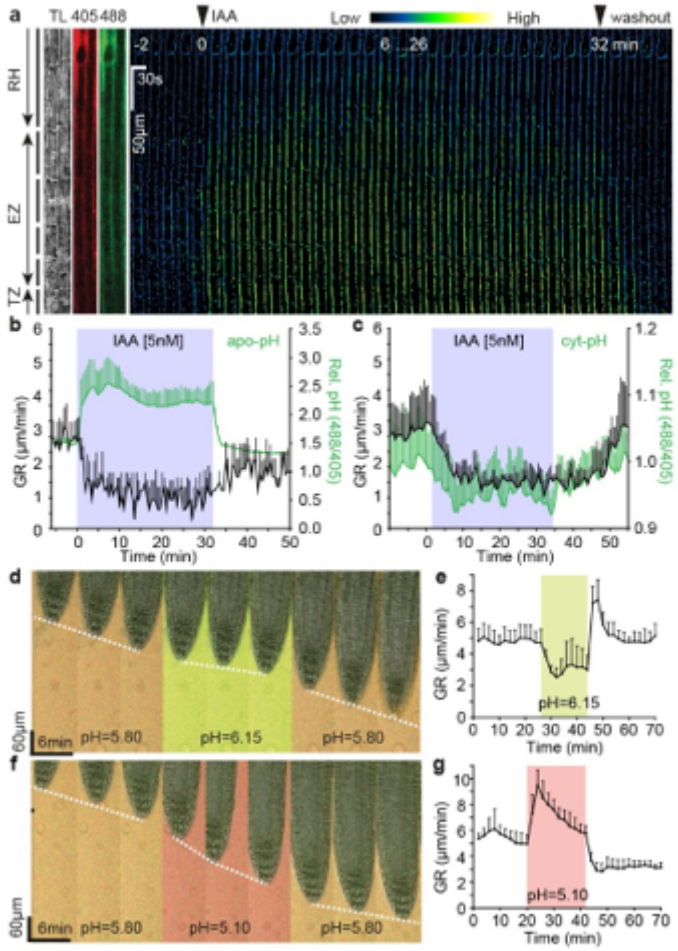

Figure 1

Auxin rapidly inhibits root growth by apoplast alkalinisation. a, Time-lapse of apoplastic pH in 5nM IAA treated root tip epidermal cells followed by washout in vRootchip. Ratiometric image (488nm/405nm) of HPST staining to monitor pH in Root hair (RH), elongation (EZ) and transition zone (TZ). TL is transmitted light. b, Quantification of apoplastic pH and growth rate (GR) in the EZ following 5nM IAA and washout as in (a). Mean of 4 roots+SD. c, Quantification of cytosolic pH (using PM-Cyto reporter) and GR in the EZ upon 5nM IAA in vRootchip. Mean of 3 roots+SD. d-g, Root growth response to alkaline (pH 6.15) (d) or acidic medium (pH 5.10) (f). The white dotted line tracks the root tip over time. Quantifications of GR in d (n=8 roots) (e) and f (n=7 roots) (g). Shaded areas represent the duration of treatments. Mean+SD.

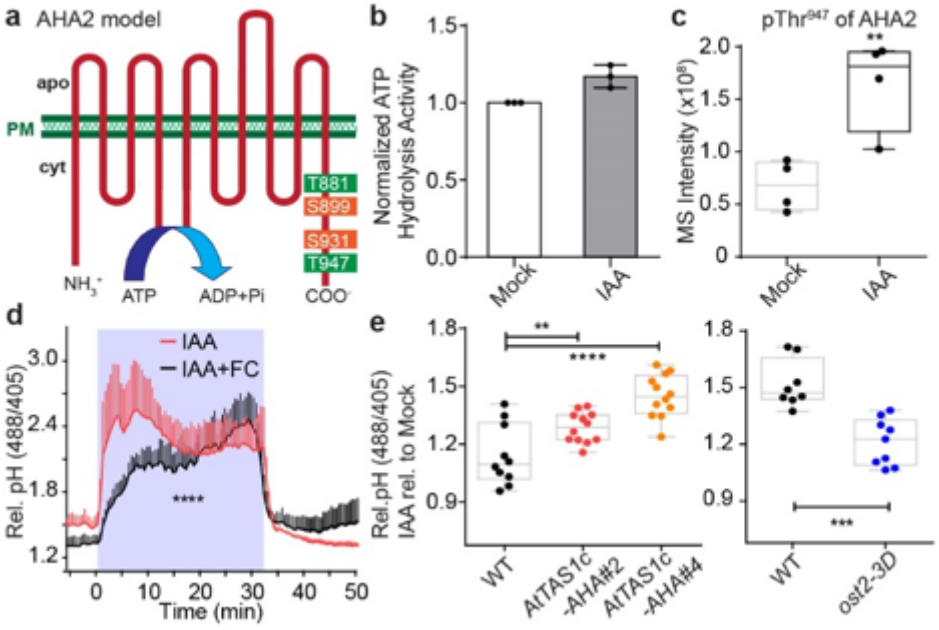

Figure 2

Auxin-triggered H+-ATPase activation counteracts auxin-triggered apoplast alkalinisation. a, AHA2 phospho-sites identified in the phospho-proteomic analysis of roots after 2min of 100nM IAA. Green reflects activation and orange inhibition of H+-translocation. b, Quantification of ATP hydrolysis in roots treated 1h with 100nM IAA normalized to mock. Bars indicate mean of 3 biological replicates+SD. Unpaired t-test, *p=0.0138. c, Thr947-phosphorylation of AHA2 in roots after 2min 100nM IAA treatment. n= 4 biological replicates. Box plot depicts minimum to maximum, mean±SD. Unpaired t-test, **p=0.0077. d, Activation of H+-ATPases by 10µM FC affected 10nM IAA-induced alkalinisation. The shaded area represents the duration of the treatment. Mean of 4 roots+SD. ****p≤0.0001 from 0–32min, Two-way ANOVA. e, Apoplast alkalinisation in AtTAS1c-AHA#2 and #4 (n>9 roots) and ost2-3D gain-of-function roots (n>5 roots) after 30min 5nM IAA normalized to Mock. Box plots depict minimum to maximum, mean±SD. **p≤0.01, ***p≤0.001, ****p≤0.0001, One-way ANOVA.

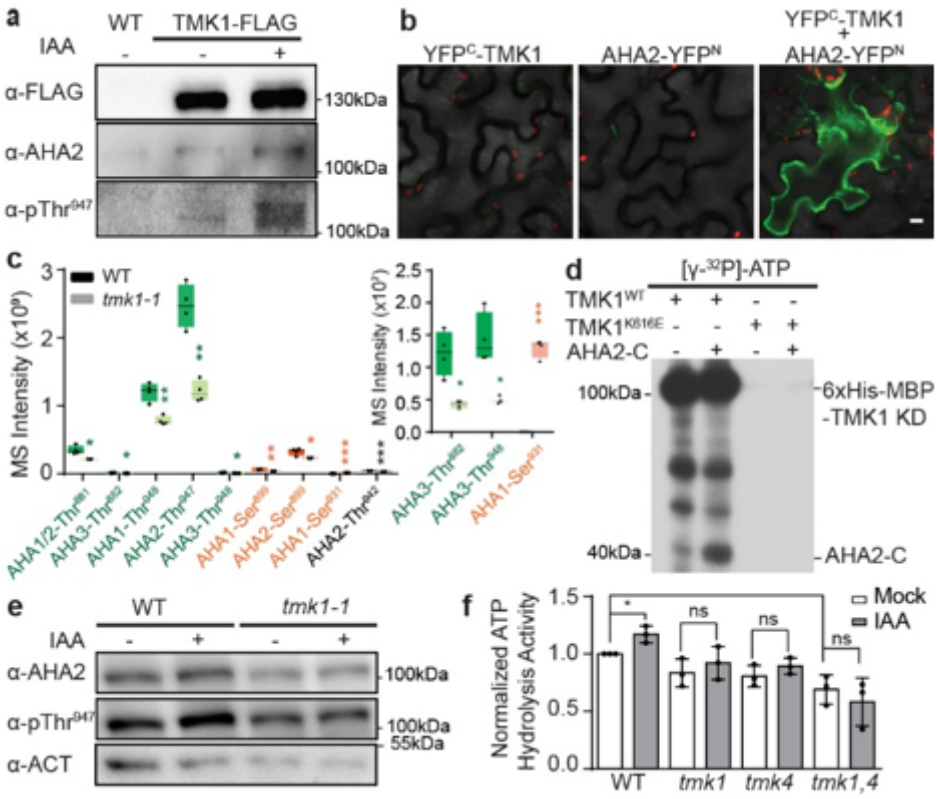

Figure 3

TMK1 directly mediates auxin-induced H+-ATPase activation. a, Co-immunoprecipitation (co-IP) of pTMK1::TMK1-FLAG roots after 30min 100nM IAA, followed by Western blot detection of AHA2 and pThr947-AHA2. b, Bimolecular Fluorescent Complementation (BiFC) in Nicotiana benthamiana leaves transiently transformed either with YFPC-TMK1, AHA2-YFPN or both. Scale bar=10μm. c, Phospho-sites of AHAs in tmk1-1 and WT. Green indicates known activation, orange inhibitory, and grey unknown function. The smaller insert shows sites with lower detected values. n=4 biological replicates, Box plot depicts minimum to maximum, mean±SD. Student t-test, *p≤0.05,**p≤0.01,***p≤0.001. d, In vitro kinase assay with [γ -32P]-ATP, C-terminal AHA2 (AHA2-C) and the kinase domain of TMK1WT or kinase dead TMK1K616E. AHA2-C is phosphorylated by TMK1WT and not by TMK1K616E. Autophosphorylation of TMK1WT is also detected. e, Western blot analysis of AHA2 Thr947 phosphorylation in WT and tmk1-1 roots treated 1h with 100nM IAA. f, Auxin-induced ATP hydrolysis activity is impaired in tmk mutants (1h 100nM IAA). Levels were normalized to mock-treated WT. Mean of 3 biological replicates+SD. *p≤0.05, ns p>0.05, One-way ANOVA.

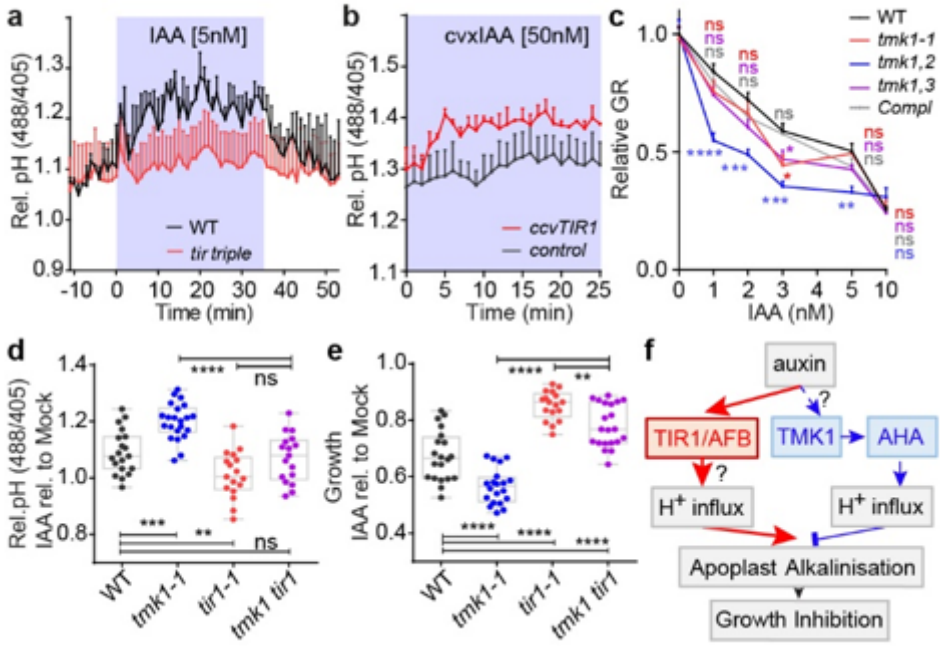

Figure 4

Antagonistic TIR1/AFB and TMK1 signalling converge on apoplastic pH for growth regulation. a, Apoplastic pH response in tir triple mutant (red) compared to WT roots (black) in vRootchip. Mean of 3, 2 roots+SEM. b, Apoplastic pH analysis in ccvTIR1 (red) compared to control (black) in response to cvxIAA in vRootchip. Mean of 2, 3 roots+SEM. Shaded area represents duration of treatment. c, Dose-response of root growth inhibition of tmk1-related mutants and pTMK1::TMK1-FLAG in tmk1-1 (Compl). Relative growth is the ratio of auxin to mock GR in the same genotype. n>15 roots. *p≤0.05, **p≤0.01, ***p≤0.001, ****p≤0.0001, Welch ANOVA. d-e, Apoplastic pH (d) and root growth (e) measurement in tmk1-1, tir1-1 and tmk1 tir1 mutants in response to 5nM IAA for 50min (d) and 6h (e). n>16 roots. Box plot depicts minimum to maximum, mean±SD. ns p>0.05, **p≤0.01, ***p≤0.001, ****p≤0.0001, one-way ANOVA. f, Model for auxin-induced root growth regulation. An intracellular, non-transcriptional branch of TIR1/AFB signalling pathway (red) mediates rapid H+-influx for apoplast alkalinisation and growth inhibition. Cell surface TMK1 activates H+-pumps (AHAs) (blue) to acidify apoplast and promote growth.

Supplementary Files

This is a list of supplementary files associated with this preprint. Click to download.

- ExtendedData.docx
- ExtendedDataTable1phosphositesAHAs.xlsx
- ExtendedDataTable2TIR1AFB1IPMS.xlsx
- ExtendedDataTable3TMK1IPMS.xlsx
- ExtendedDataTable4primers.xlsx